Ecological Informatics 95 (2026) 103744

Contents lists available at ScienceDirect

Ecological Informatics

journal homepage: www.elsevier.com/locate/ecolinf

Integrating spectral, textural, and topographic features for ecological forest type classification with XGBoost

Richard Kovárník *, David Hampel, Jitka Janová

Department of Statistics and Operation Analysis, Faculty of Business and Economics, Mendel University in Brno, Zemědělská 1, 61300 Brno, Czech Republic

ARTICLE INFO

Keywords:
Forest site classification
Multimodal remote sensing
Vegetation indices
Temperate forests
Extreme gradient boosting
Machine learning

ABSTRACT

Forests play a critical role in ecological stability and resource management, and their sustainable management increasingly relies on advanced remote sensing and data-driven approaches. In this study, we evaluate the potential of multimodal satellite data for detailed ecological forest site type classification within a heterogeneous forested region of the Czech Republic. We compiled a comprehensive dataset of 156 features integrating Sentinel-2 multispectral bands, Sentinel-1 SAR backscatter, vegetation indices, seasonal median composites, texture metrics, topographic variables, and a high-resolution canopy height model. Using this feature set, an Extreme Gradient Boosting (XGBoost) classifier was trained to map 16 ecological forest site type groups, dominated by rich/enriched beech–oak forests, beech–oak forests, and loamy oak–beech forests. The model achieved an overall accuracy of 88.4% and a macro-averaged F1-score of 0.89, with the highest classification performance obtained for fir forests, other beech forests, and calcareous forest types. Feature importance analysis shows that radar texture features, seasonal vegetation indices, and topographic variables are among the most influential predictors, while canopy height texture metrics further enhance class separability. These results demonstrate that combining diverse remote sensing modalities with advanced machine learning enables reliable, fine-scale mapping of complex ecological forest site types, extending beyond traditional tree-species classification and offering a scalable and cost-effective tool for ecological research and forest management planning.

1. Introduction

Forests represent some of the most complex and valuable terrestrial ecosystems on Earth, playing a fundamental role in global carbon sequestration, water regulation, soil stabilization, and biodiversity conservation (FAO, 2024; Miura et al., 2015). Beyond these ecological services, forests also support economic and cultural values central to human societies. However, rapid environmental change, including climate variability, invasive pests, and anthropogenic pressures, has made sustainable forest management increasingly challenging (Seidl et al., 2017). A key to addressing these challenges lies in accurately mapping and monitoring forest ecosystems over time. Traditional field-based surveys, while precise, are often costly, time-consuming, and limited in spatial coverage (Fassnacht et al., 2016). Consequently, the adoption of remote sensing technologies has become essential in modern forestry and ecological research (Hansen et al., 2013). Remote sensing provides repeatable, objective, and spatially extensive observations that support decision-making at multiple scales — from stand-level silvicultural planning to national forest inventories (Wulder et al., 2019).

Remote sensing, as applied to forest monitoring, spans a diverse range of technologies, including unmanned aerial vehicles (UAVs), airborne laser scanning, and spaceborne sensors. Satellite-based observations, particularly from open-access missions such as Sentinel-1, Sentinel-2, Landsat, and MODIS, have been widely embraced due to their frequent revisit times and consistent global coverage (Astola et al., 2019; Kovárník and Janová, 2025; Kowalski et al., 2020). Sentinel-2, for example, offers high-resolution multispectral data that can distinguish subtle differences in canopy reflectance, while Sentinel-1 provides synthetic aperture radar (SAR) data valuable for capturing structural attributes of forests even under cloud cover (Fang et al., 2023). The integration of multispectral and radar data, along with derived products such as vegetation indices (e.g., NDVI, EVI), canopy height models, and texture metrics, has shown promise in enhancing classification accuracy, particularly in heterogeneous landscapes (Fassnacht et al., 2016; Song et al., 2021). These multimodal datasets can capture both biochemical and structural characteristics of forest stands, which are critical for detailed ecological mapping (Kozhoridze et al., 2016).

Despite substantial advances in remote sensing data availability and

* Corresponding author.
E-mail addresses: xkovarn1@mendelu.cz (R. Kovárník), david.hampel.uso@mendelu.cz (D. Hampel), jitka.janova@mendelu.cz (J. Janová).

https://doi.org/10.1016/j.ecoinf.2026.103744
Received 24 September 2025; Received in revised form 25 March 2026; Accepted 25 March 2026
Available online 27 March 2026

machine learning algorithms, forest type classification in practice remains largely limited to relatively broad categories—such as coniferous versus broadleaved forests or dominant tree species. This limitation is driven by persistent challenges, including insufficient and spatially uneven ground truth data, high within-class variability caused by stand age, management, and structural heterogeneity, as well as overlapping spectral signatures among temperate mixed-forest species and site conditions (Kovárník and Janová, 2025; Pu, 2021). Consequently, many recent studies still focus on assigning forest areas to coarse tree-species groups. For example, Ma et al. (2021) classified a forest region into 4 species categories using Sentinel-2 multispectral bands, while Mohammadpour et al. (2022) mapped Portuguese forests into 6 dominant tree species classes alongside four general land-cover types such as cropland and water. Even studies that employ multi-sensor fusion—such as Wan et al. (2021), who combined multispectral, SAR, and environmental variables—typically target fewer than a dozen species, achieving high accuracy (≈0.9) but still operating at a coarse taxonomic level. In contrast, a study in Arkansas, USA, first applied a Random Forest classification to Sentinel-2 imagery and then refined the results using secondary modeling approaches to produce a detailed map of 123 ecological system types, including forests, plantations, and cultural vegetation classes (Sunde et al., 2024).

In this study, we focus on the Masaryk Forest Křtiny in the Czech Republic, a complex and ecologically valuable landscape comprising diverse forest types influenced by soil properties, hydrology, and historical management practices. Our goal is to classify this area into 16 ecologically meaningful forest categories. These categories reflect key ecological gradients such as soil fertility, moisture availability, and geomorphological conditions, which in turn influence the natural potential species composition and forest dynamics. Such a typology aligns with the official Czech forest typological system, which is widely used to guide sustainable silviculture and conservation planning (Viewegh, 2012). To achieve this detailed classification, we constructed a multimodal dataset by combining Sentinel-2 multispectral data, Sentinel-1 SAR data, vegetation indices (e.g., NDVI, NDWI), topographic variables (elevation, slope, aspect), texture features derived from gray-level co-occurrence matrices (GLCM), and canopy height information. The classification was performed using an Extreme Gradient Boosting (XGBoost) model, an ensemble machine learning algorithm known for its robustness to noise, ability to handle complex interactions, and relatively low sensitivity to parameter tuning (Zhao et al., 2023). Our workflow is designed to address two core research questions: (i) whether multimodal environmental and remote-sensing data are capable of reliably distinguishing among ecologically defined forest types, and (ii) which predictors contribute most strongly to model performance and thus best capture the underlying ecological gradients.

Our study contributes to the growing field of ecological informatics in several ways. First, it demonstrates the utility of freely available, high-resolution satellite data for producing ecologically nuanced forest maps, even in complex temperate landscapes. Second, it offers a reproducible workflow that can be adapted to other forested regions. Third, it provides an open reference dataset, which may help address the persistent bottleneck of limited ground truth data in remote sensing research. Ultimately, such detailed forest type maps can support a range of applications, including forest vulnerability assessments or adaptive management planning. In summary, integrating multispectral, radar, and ecological data, combined with robust machine learning approaches, enables a deeper understanding of forest heterogeneity. This work illustrates how machine learning can bridge the gap between satellite observations and actionable insights for sustainable forest management.

2. Material and methods

2.1. Study area

The School Forest Enterprise Masaryk Forest Křtiny is a university-owned forest estate managed by Mendel University in Brno, Czech Republic. Established in 1923, it is located in the Drahanská Highlands near the town of Křtiny (latitude 49°15′ N, longitude 16°15′ E), approximately 20 km northeast of Brno (Fig. 1). Covering an area of roughly 10,200 hectares, the enterprise serves as a multifunctional forest, balancing sustainable timber production with biodiversity conservation, soil and water protection, and landscape management. The altitude ranges from 210 to 575 m, with a mean annual temperature of 7.5 °C and average annual precipitation of around 610 mm. The area features diverse natural geomorphological conditions. The forest stands consist of approximately 54% broadleaved and 46% coniferous species, with the five most dominant being European beech (*Fagus sylvatica*), Sessile oak (*Quercus petraea* agg.), Norway spruce (*Picea abies*), Scots pine (*Pinus sylvestris*), and European hornbeam (*Carpinus betulus*) (Mašínová et al., 2017). The area encompasses diverse soil types, including luvisols, fluvisols, and gleysols (Hammond et al., 2020).

The Masaryk Forest is classified according to the official forest type classification system of the Czech Republic (Decree No. 298/2018 Coll., on the preparation of regional forest development plans and the definition of forest management units). This system defines sets of forest types as the basic units of forest typology, grouping forest types based on ecological similarity and habitat characteristics relevant for forest management. The classification follows the principles described by (Viewegh, 2012), who characterizes forest types as ecologically coherent units defined by shared environmental conditions.

Each forest type category is characterized by a combination of attributes: absolute height site productivity classes (AVB), soil type and subtype, substrate, relief, slope, exposure, natural species composition, soil depth, and elevation above sea level.

Within the Masaryk Forest, there are originally 57 distinct forest types. For the purpose of machine learning classification, we grouped them into 16 broader forest type categories (Fig. 2) based on ecological similarity, as the original classification was too detailed to be practical for modeling. The aggregation was based on diagnostic ecological descriptors contained in the official typology names—specifically key indicators of soil substrate and chemistry (e.g. loamy, calcareous, acidic), moisture regime (e.g. wet, waterlogged, drying), trophic status (rich vs. mesotrophic), relief and soil depth (skeletal, stony, dwarf forms), and dominant tree-species composition (beech–oak, oak–beech, fir–-broadleaved). The structure of individual target classes used for model training is presented in Table 1. Since this study involves real ecological data, it is important to acknowledge that the target classes are highly imbalanced, as illustrated in Fig. 3. Such imbalance is common in ecological datasets due to the natural variability and uneven distribution of forest types across the landscape. Addressing this class imbalance is critical for ensuring robust model performance and avoiding bias toward the more prevalent classes.

The study area encompasses a diverse mosaic of forest communities with specific species composition, soil, and hydrological conditions. Loamy forests occur on fertile, well-drained loess soils and are dominated by mixtures of oak and beech. Mesotrophic broadleaved forests occupy moderately fertile sites and include diverse deciduous assemblages such as oak–hornbeam, lime–maple, maple–ash, and mixed oak–beech forests. Drying forests develop on drier, well-drained slopes, typically consisting of oak–beech or beech–oak stands. Oak–beech forests represent fresh, moderately fertile sites where oak and beech co-dominate, sometimes with maple admixture. Other forests include relict pine stands and minor unclassified communities.

Rich or enriched forests are nutrient-rich, species-diverse beech–oak or beech-dominated forests, reflecting high site fertility. Beech–oak forests grow on moderately fertile soils with varying contributions of

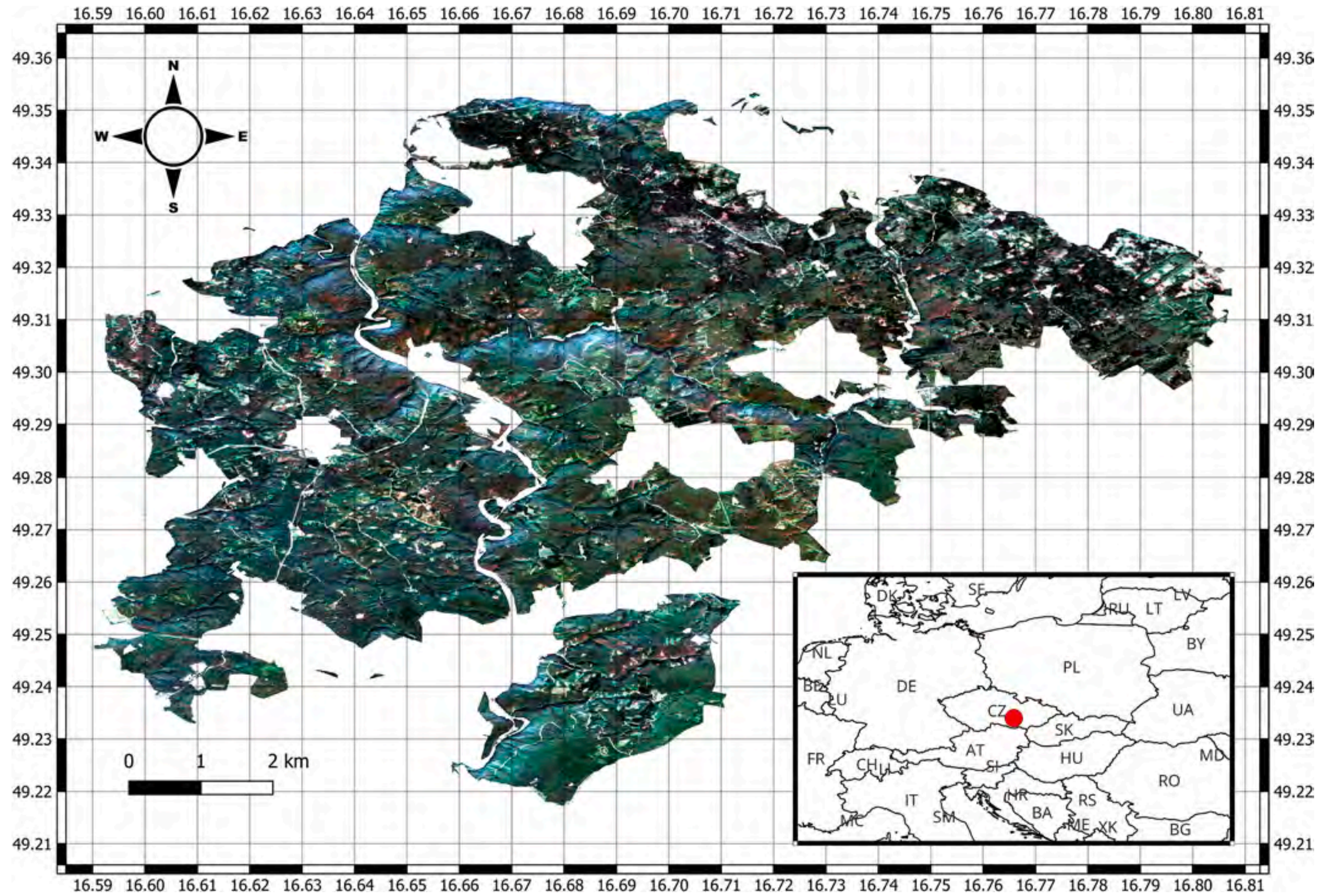

Fig. 1. The location of Masaryk Forest in Křtiny, Czech Republic (study area, Sentinel 2 RGB composite)

oak, beech, lime, or fir. Other beech forests are generally monospecific or nearly monospecific stands on nutrient-poor soils. Fir forests occupy cool, moist slopes or ravines where fir co-occurs with beech.

Calcareous forests develop on limestone substrates and are rich in calciphilous species. Acidic forests occur on nutrient-poor, acidic soils, including stony variants. Skeletal, stony, or dwarf forests grow on shallow, rocky soils or steep slopes, often forming stunted stands. Waterlogged or streamside forests occupy sites with high soil moisture, along streams, or in wet depressions, and include willow–alder carrs. Riparian or floodplain forests are dominated by ash–alder communities on periodically inundated soils. Wet forests develop on persistently moist sites, with beech and oak as the main canopy species. Finally, Cornelian cherry forests are characterized by the presence of Cornelian cherry in association with beech and oak, forming unique mixed stands.

2.2. Remote sensing data

For the purpose of performing supervised classification into the above-mentioned target classes, we compiled a comprehensive multimodal dataset containing a total of 156 features. These include a 1 m canopy height model (Tolan et al., 2024), Sentinel-2 multispectral bands (blue, green, red, red-edge, near-infrared, and shortwave infrared), Sentinel-1 backscatter features (VV and VH polarizations and their ratios and differences), derived vegetation indices, seasonal median composites and temporal heterogeneity metrics (e.g., NDVI percentiles and standard deviation), GLCM texture features computed from canopy height, NDVI, VV, and VH, and topographic variables derived from NASA SRTM digital elevation data (elevation, slope, and aspect). We selected the canopy height model from (Tolan et al., 2024) because it provides a recent, high-resolution product trained using aerial lidar and GEDI observations, making it particularly suitable for fine-scale forest site classification. All remote sensing features were extracted and processed using Google Earth Engine (Gorelick et al., 2017). An aggregated overview of the input feature groups is presented in Table 2.

Satellite data were aggregated both annually and seasonally to account for temporal variability in forest canopy and vegetation. Sentinel-2 surface reflectance images were filtered for the year 2020 and masked for clouds using the Scene Classification Layer (SCL); annual median values as well as seasonal medians (spring: Mar–May, summer: Jun–Aug, autumn: Sep–Nov) were computed for all spectral bands and derived vegetation indices. Sentinel-1 SAR data (VV and VH polarizations) were similarly filtered for 2020, merged across ascending and descending orbits, and median composites were created for annual and seasonal periods. The 1 m Canopy Height Model represents conditions from 2018 to 2020. All datasets were resampled to a uniform 10 m resolution for supervised classification. Google Earth Engine performs nearest-neighbor resampling by default during reprojection. For continuous variables (CHM, Sentinel-2 and Sentinel-1 bands, vegetation indices, and texture features), nearest-neighbor resampling preserves the original pixel values but may slightly reduce smoothness of fine-scale heterogeneity. The complete list of individual features, along with detailed descriptions, is provided in the `band_descriptions.py` (see the GitHub repository referenced below). To ensure temporal consistency with the Canopy Height Model (which primarily represents conditions from 2018 to 2020), we used remote sensing data acquired from the year 2020.

All 156 input features were extracted for the entire area of the Masaryk Forest and exported as a single multiband GeoTIFF with a

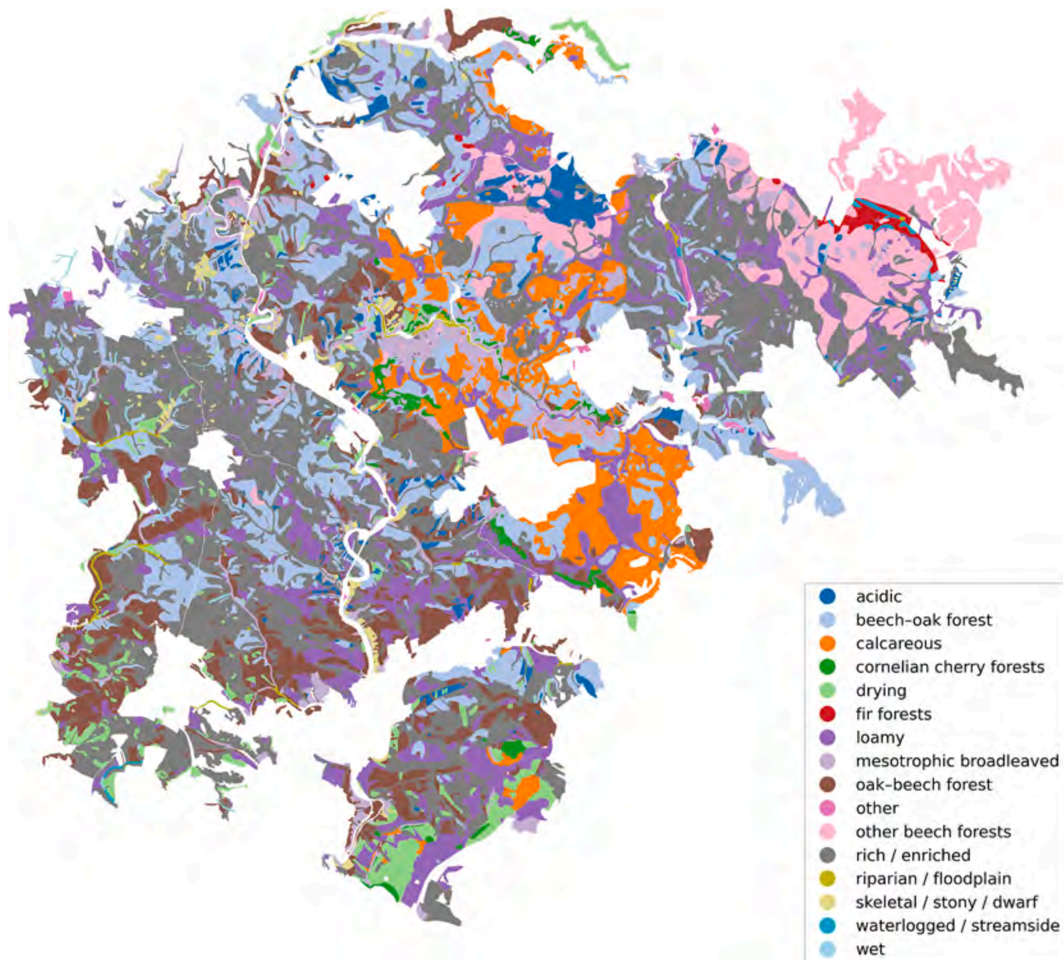

Fig. 2. Forest site type classification (target classes) in the Masaryk Forest

spatial resolution of 10 m. Each pixel carries a set of multimodal predictors, including spectral reflectance, vegetation indices, radar backscatter, texture metrics, canopy height, and topographic attributes, serving as input for supervised classification into forest site types. Finally, the raster file was spatially joined with the shapefile containing the target classification. This integration produced an additional feature representing the target class label for each pixel in the raster dataset.

Out of all 156 bands, there are 4 bands with no values at all, while the vast majority of the remaining bands have the same number of missing values (see Fig. 4). This pattern suggests that there is a specific part of the study area for which data were unavailable. Such gaps are common in remote sensing datasets and can occur for various reasons, including cloud cover, clipping data to the area of interest, or merging target vector data with raster layers.

The four bands with missing data are bands 98, 116, 134, and 152. These bands represent Maximal Correlation Coefficient texture features derived from canopy height, NDVI, and Sentinel-1 VV and VH. The Maximal Correlation Coefficient texture bands can have missing values because this metric requires sufficient variation within the pixel window to compute meaningful correlations. In areas where the input data is uniform or nearly constant, or where data is masked or incomplete, the calculation becomes undefined, resulting in missing values. This is a common issue with complex texture measures, especially when using small window sizes or when input data contains gaps. Due to the absence of valid values, these bands will be excluded during the creation of the classification model.

2.3. Supervised classification

We developed a reproducible machine learning pipeline to classify forest types using multi-band raster data. The pipeline was implemented in Python and integrates data preprocessing, feature engineering, class balancing, model training, and comprehensive performance evaluation. All experiments were performed in Python, using open-source libraries: XGBoost (Chen and Guestrin, 2016), scikit-learn, NumPy, pandas, Matplotlib, seaborn, and rasterio and geopandas for geospatial data handling. The code, including preprocessing, modeling, and visualization scripts, is made available in the GitHub repository listed in the Data Availability section to ensure reproducibility.

2.3.1. Model architecture and training

We used Extreme Gradient Boosting (XGBoost), a state-of-the-art gradient boosting framework known for its scalability and superior predictive accuracy in structured data tasks (Brownlee, 2016; Chen and Guestrin, 2016). XGBoost has proven to be highly effective for remote-sensing applications. Bhagwat and Shankar (2019) demonstrated that it outperforms several traditional machine-learning algorithms, including Random Forest and Naïve Bayes. Similarly, Zhou et al. (2022) reported that XGBoost offers superior performance during training and faster computational speed compared to Support Vector Machines, while also achieving higher classification accuracy than the Spectral Angle Mapper (SAM). In addition, Kwenda et al. (2023) compared Random Forest, XGBoost, deep-learning models and their combinations for remote-sensing forest classification and found that XGBoost achieved the highest accuracy, further underscoring its strong potential for

Table 1
Structure of ecological forest types for machine learning classification

ID	Name	Forest types
1	loamy	Loamy (loess) oak–beech forest; Loamy beech–oak forest; Loamy beech forest
2	mesotrophic broadleaved	Dry oak–hornbeam forest; Lime–maple forest; Maple–ash forest; Maple–hornbeam oak–beech forest; Rich oak–hornbeam oak–beech forest; Loess oak–hornbeam forest; Lime beech forest; Maple–hornbeam oak–beech forest
3	drying	Drying oak–beech forest; Drying beech–oak forest
4	oak–beech forest	Fresh oak–beech forest; Maple–beech oak–beech forest
5	other	Relict pine forest; Not classified
6	rich/enriched	Enriched beech–oak forest; Rich beech forest; Rich oak–beech forest; Enriched oak–beech forest; Enriched beech forest; Rich oak–beech forest
7	beech–oak forest	Fresh beech–oak forest; Lime–oak beech forest; Fir–oak beech–oak forest
8	other beech forests	Fresh beech forest; Dealpine beech forest
9	fir forests (mixed fir–broadleaved forests)	Fresh beech fir forest; Fresh (beech) fir forest
10	calcareous	Calcareous beech–oak forest; Calcareous beech forest; Calcareous oak–beech forest
11	acidic	Acidic oak–beech forest; Acidic beech–oak forest; Stony acidic beech–oak forest; Stony acidic oak–beech forest; Acidic beech forest; Acidic oak forest
12	skeletal/stony/dwarf	Stunted oak–beech forest; Stunted oak forest; Stunted beech–oak forest; Slope beech–oak forest; Skeletal beech–oak forest; Fresh stony oak–beech forest
13	waterlogged/streamside	Waterlogged fir–oak beech–oak forest; Waterlogged fir forest; Waterlogged fir–oak beech–oak forest (upper stage); Streamside riparian forest; Willow–alder carr
14	riparian/floodplain	Ash–alder carr
15	wet	Wet beech–oak forest; Wet beech forest; Wet oak–beech forest
16	cornelian cherry forests	Cornelian cherry beech forest; Cornelian cherry oak forest; Cornelian cherry oak forest with beech

remote-sensing–based mapping and analysis.

XGBoost builds an ensemble of decision trees in a stage-wise fashion, minimizing a differentiable loss function via gradient descent while incorporating regularization to reduce overfitting and improve generalization (Friedman, 2001). The model can be accelerated with GPU computing to handle large-scale geospatial data efficiently.

The dataset was initially split into training (80%) and testing (20%) subsets using stratified sampling to preserve class distributions. Lastly, k-fold cross-validation was used to obtain more robust results. Initial hyperparameters (e.g., `max_depth, eta`) were selected based on best practices from the literature and refined manually, as automated hyperparameter search (e.g., randomized search) proved computationally intensive on the available infrastructure.

The input consisted of multi-band GeoTIFF rasters containing raw spectral data, textural features, and vegetation indices derived from remote sensing. The target variable (forest type) was extracted from a separate band, while non-forest or masked areas were excluded. To reduce dimensionality and prevent multicollinearity, we applied variance thresholding to remove zero-variance features. Although principal component analysis (PCA) was tested, it did not improve model performance and was therefore omitted since tree-based models often handle multicollinearity robustly.

Table 2
Main feature categories and selected examples from the complete feature list.

Group	Bands/Feature Example	Description	Original Resolution
Sentinel-2 spectral bands	B2, B3, B4, B5, B6, B7, B8, B8A, B11, B12	Blue, Green, Red, NIR, SWIR, and red edge bands.	10–20 m
Vegetation indices	NDVI, EVI, NBR, NDWI, etc.	Standard and red edge indices characterizing vegetation greenness, water content, and stress.	10–20 m
Seasonal median indices	spring_NDVI, summer_NDVI, autumn_NDVI etc.	Seasonal summaries to capture phenology.	10–20 m
Sentinel-1 radar	VV, VH, ratios, seasonal medians etc.	Backscatter to describe structure and moisture.	10 m
Topography (NASA SRTM DEM)	elevation, slope, aspect	Terrain properties.	30 m
Texture features	GLCM statistics of Canopy height, NDVI, VV, VH etc.	Texture measures describing spatial variation.	Same as input data
Percentile & variability	NDVI_p90, NDVI_stdDev etc.	Temporal heterogeneity.	10–20 m
Canopy height	Canopy height (m)	Global canopy height product.	1 m

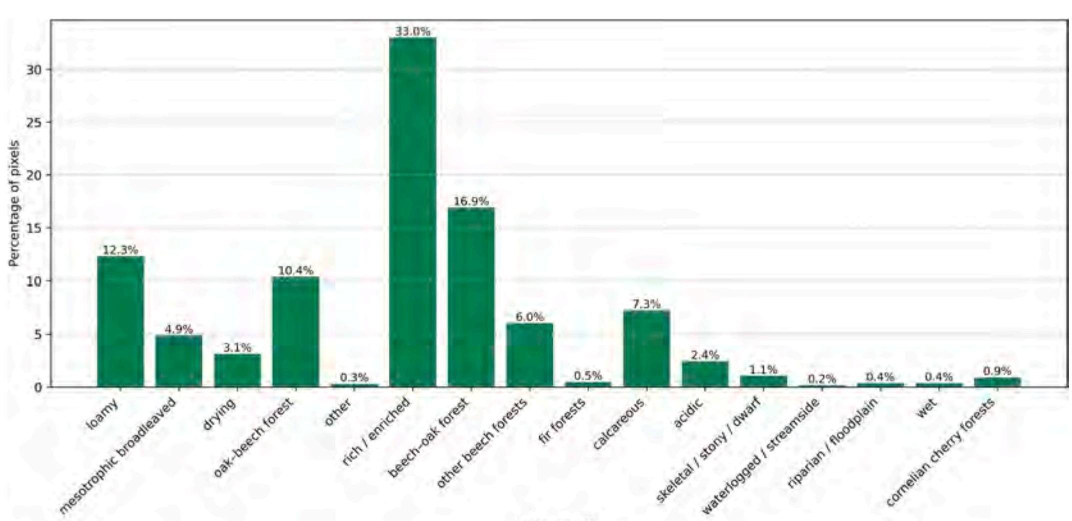

Fig. 3. The percentage of pixels for each forest type category in the Masaryk Forest

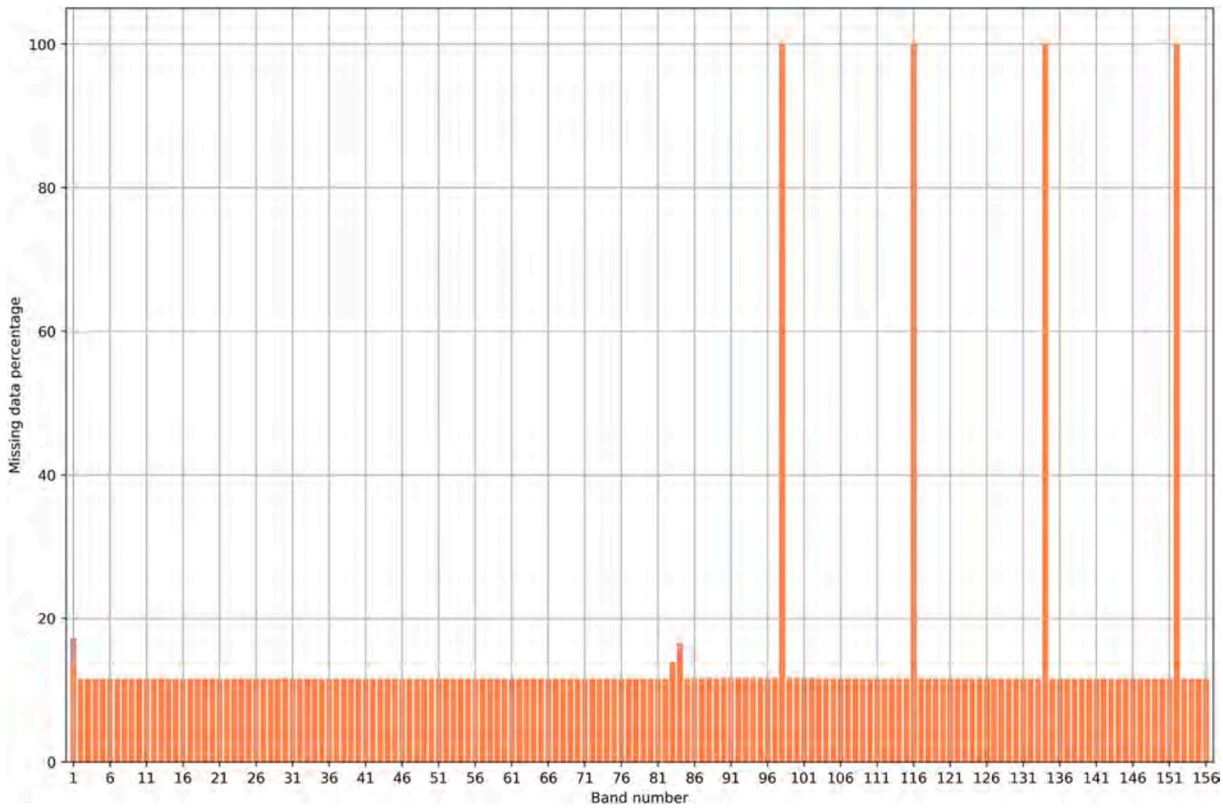

Fig. 4. Missing values by each feature (band) in the dataset.

Missing data were handled conservatively: rows with missing values were excluded, since large spatial gaps made imputation strategies (e.g., mean imputation) unsuitable and potentially misleading. To mitigate class imbalance, per-class sample weights inversely proportional to class frequencies were calculated, following established practice for imbalanced classification tasks (He and Garcia, 2009; Kaur et al., 2019).

2.3.2. Performance evaluation

Model performance was assessed comprehensively by computing overall accuracy together with macro- and weighted-average precision, recall, and F1-score to capture both overall and class-specific performance. To evaluate the discriminative ability of the classifier, we generated ROC curves and calculated per-class ROC AUC scores, while also reporting the macro-averaged ROC AUC to provide a single summary metric. In our multi-class setting, we applied the One-vs-Rest approach, in which each forest type class is treated as the positive class while all other classes are considered negative. Precision-recall curves were included to further explore performance, especially in the context of class imbalance.

To quantify the agreement between predicted and true labels beyond chance, we computed Cohen's kappa coefficient (Cohen, 1960). Model calibration was assessed both quantitatively, using the multi-class Brier score as a measure of probabilistic accuracy (Glenn et al., 1950), and visually, through calibration plots showing the correspondence between predicted probabilities and observed frequencies (Niculescu-Mizil and Caruana, 2005). Additionally, confusion matrices were used to illustrate misclassification patterns across classes, and feature importance scores based on gain were examined to interpret the relative contribution of individual predictors to the model's decisions. To assess robustness and reduce overfitting risk, we repeated model training under a 5-fold cross-validation scheme. This provided mean and standard deviation of metrics across folds, confirming stability of the results. The steps undertaken in the study are summarised in Fig. 5.

3. Results

The classification results (Table 3) show an overall accuracy of 88.4%, with macro-averaged precision, recall, and F1-scores of 0.8904, 0.8946, and 0.8919, respectively. Weighted averages, which account for the distribution of classes in the dataset, are slightly lower yet consistent (precision: 0.8852, recall: 0.8840, F1-score: 0.8839). Support (no. of test pixels) indicates the number of test samples (pixels) belonging to each forest type class that were used to compute the corresponding.

Per-class performance indicates generally strong predictive capability across most forest types. The highest F1-scores are observed for fir forests (0.9507), other beech forests (0.9150), and cornelian cherry forests (0.9130). Loamy forests and mesotrophic broadleaved forests also achieve solid F1-scores of 0.8602 and 0.8965, respectively, reflecting balanced precision and recall.

Notably, oak–beech forests achieve high recall (0.931) but comparatively lower precision (0.8299), resulting in an F1-score of 0.8775, suggesting the model tends to overpredict this class. Conversely, the "wet" forest type has the lowest F1-score (0.7958), driven by relatively low recall (0.7521). Despite these variations, performance across most classes remains robust, especially for dominant types with larger support, such as rich/enriched forests (F1-score: 0.8832) and beech–oak forests (F1-score: 0.8709).

The confusion matrix (Fig. 6) demonstrates generally strong agreement between predicted and actual classes, reflected by the high counts along the main diagonal. Larger forest types with substantial representation, such as rich/enriched forests (class 6), beech–oak forests (class 7), and loamy forests (class 1), show high numbers of correctly classified samples. Even smaller or rarer classes, including cornelian cherry forests (class 16) and fir forests (class 9), retain relatively high correct prediction rates compared to their total support, which indicates the model's capacity to identify less common types.

Most misclassifications occur between classes that share similar ecological or spectral characteristics, typically those dominated by

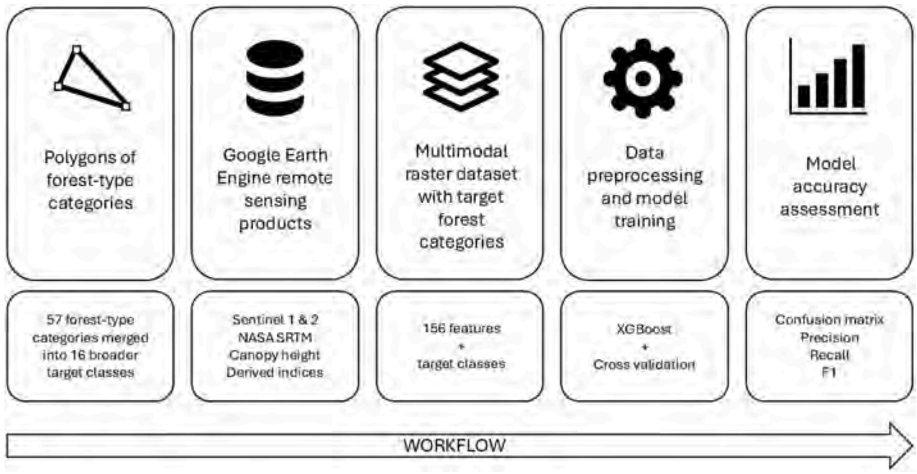

Fig. 5. Methodological steps undertaken in the study.

Table 3
Accuracy assessment for XGBoost classification model.

ID	Name	Precision	Recall	F1-score	No. of test pixels
1	loamy	0.8767	0.8443	0.8602	38421
2	mesotrophic broadleaved	0.9053	0.8878	0.8965	14542
3	drying	0.9132	0.8997	0.9064	8886
4	oak–beech forest	0.8299	0.9310	0.8775	31313
5	other	0.9412	0.9464	0.9438	541
6	rich/enriched	0.9077	0.8599	0.8832	107192
7	beech–oak forest	0.8629	0.8790	0.8709	53762
8	other beech forests	0.8707	0.9640	0.9150	15797
9	fir forests	0.9431	0.9584	0.9507	1419
10	calcareous	0.8933	0.9398	0.9159	22026
11	acidic	0.9200	0.8949	0.9073	8020
12	skeletal/stony/dwarf	0.8770	0.8905	0.8837	3396
13	waterlogged/ streamside	0.8879	0.8670	0.8773	466
14	riparian/floodplain	0.8710	0.8753	0.8732	810
15	wet	0.8448	0.7521	0.7958	948
16	cornelian cherry forests	0.9024	0.9239	0.9130	2932
Overall accuracy		0.8840			310471
macro avg		0.8904	0.8946	0.8919	310471
weighted avg		0.8852	0.8840	0.8839	310471

beech and oak tree species. For instance, rich/enriched forests (class 6) are occasionally predicted as loamy (class 1; 2,907 samples), oak-beech forest (class 4; 3,745 samples) or beech–oak forests (class 7; 4,946 samples), suggesting these classes share overlapping vegetation structure or environmental gradients captured in the spectral data. Similarly, beech–oak forests (class 7) are sometimes confused with rich/enriched forests (3,513 samples) and, to a lesser extent, loamy forests (686 samples). Oak–beech forests (class 4) show moderate confusion with loamy forests (291 samples) and rich/enriched forests (1,075 samples), which likely reflects shared mixed deciduous composition. Smaller and rarer forest types, such as waterlogged/streamside (class 13), riparian/floodplain (class 14), and wet forests (class 15), are most commonly misclassified as rich/enriched forests (class 6).

The ROC AUC scores (Fig. 7) show excellent discriminative ability across all classes, with per-class values ranging from approximately 0.97 to 1 and a high macro-averaged AUC of 0.995. These results confirm that the model reliably separates each forest type from the others, including both large and underrepresented classes, which demonstrates strong overall classification performance and robustness even in the presence of class imbalance. It should be noted, however, that these near-perfect ROC AUC scores and following PR curves reflect the model's ability to distinguish each class from all others within the study area and do not necessarily indicate its predictive performance.

The precision–recall analysis (Fig. 8) shows consistently strong performance across most classes, with average precision scores exceeding 0.90, highlighting the model's ability to balance precision and recall even under class imbalance. Only wet forests (class 15) achieve a slightly lower AP of 0.87, which still indicates reasonably good predictive quality but suggests a modest drop in the model's ability to precisely identify this minority class. Overall, these results underline the ability of the classifier to separate one class from the others. However, it should be noted that the model may demonstrate strong discriminative performance within the study area rather than true generalization to independent spatial domains.

The Cohen's kappa coefficient of 0.8583 indicates a very high level of agreement between predicted and true classes beyond chance, supporting the overall reliability of the classifier. The multi-class Brier score of 0.2094 suggests reasonably well-calibrated probability estimates (0 is perfect calibration), reflecting that predicted probabilities are generally close to the observed outcomes. Calibration plots (Fig. 9) per class further illustrate this, showing that for most classes, predicted probabilities align closely with actual frequencies, with only some deviations in some classes—especially in waterlogged/streamside forests. Due to the strong class imbalance, some classes exhibit noticeable deviations and calibration instability, which is common in ecological datasets.

The 5-fold cross-validation results (Table 4) demonstrate consistent and robust model performance across all classes, with mean precision, recall, and F1-scores generally exceeding 0.85 for most classes. Notably, classes such as 5 (other) and 9 (fir forests) show particularly high metrics, with precision and recall above 0.94, indicating strong discriminative ability. The overall accuracy remains stable at approximately 88.3%, with a low standard deviation (0.11%), suggesting minimal variability between folds and reliable generalization. Macro-averaged scores also indicate balanced performance across classes, while weighted averages reflect the influence of class distribution in the dataset. Class 15 (wet) exhibits slightly lower recall and F1, consistent with previous observations, likely due to its smaller support and greater classification challenge.

The feature importance (Fig. 10) analysis reveals that texture-related metrics from radar data, such as the average backscatter intensity (VH Sum Average) and the variance of backscatter intensity (VV Sum Variance), are among the most influential predictors. Vegetation indices capturing the greenness during the summer season (Summer GNDVI Median) also play a critical role. Additionally, terrain characteristics like elevation (SRTM Elevation) and slope (Terrain Slope) significantly contribute to the model's decisions. This combination of radar texture,

Fig. 6. Confusion matrix of XGBoost classification.

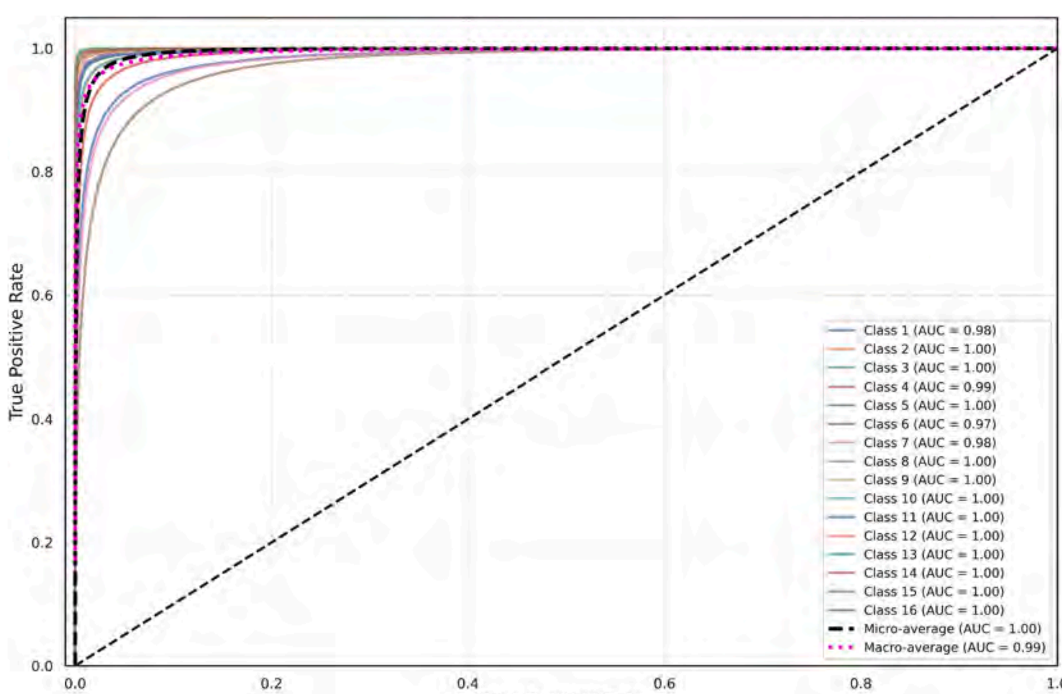

Fig. 7. One vs rest receiver operating characteristics and area under the curve values for each class.

vegetation greenness, and topographic features underscores the model's ability to integrate diverse environmental information for effective

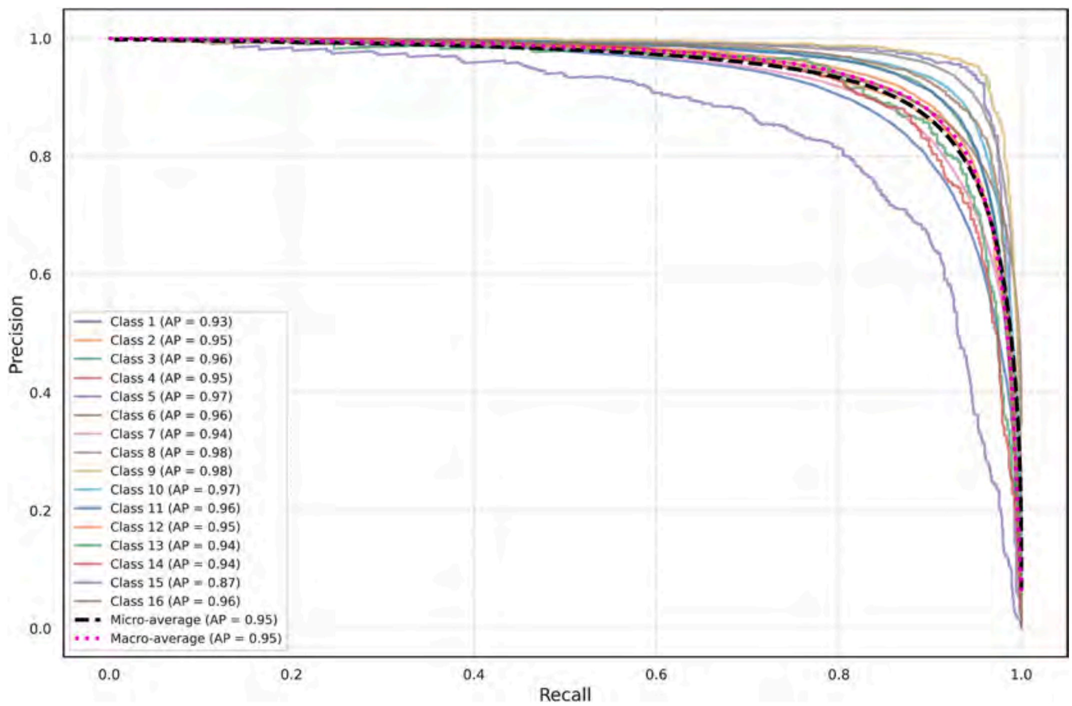

Fig. 8. One vs rest precision-recall curves for each class.

forest type classification. The full list of features is provided in `feature_importance.csv` file in the GitHub repository.

4. Discussion

The results of this study demonstrate the effectiveness of integrating multi-source remote sensing data with Extreme Gradient Boosting (XGBoost) for detailed forest type classification. Achieving high overall accuracy and strong macro-averaged ROC AUC aligns with recent findings that highlight the capability of ensemble methods and gradient boosting models in complex landscape mapping tasks (Sahin, 2020; Zhen et al., 2024). Notably, per-class performance was consistently robust, with most classes showing precision, recall, and F1-scores above 0.85, and several classes—particularly homogeneous or better-represented types such as fir forests and riparian/floodplain forests—achieving ROC AUC values above 0.90.

The overall Cohen's kappa of ≈ 0.86 indicates a substantial agreement between predicted and true classes, supporting the robustness of the classification beyond chance levels (Cohen, 1960). The multi-class Brier score (≈ 0.209) and calibration plots further indicate that the model's predicted probabilities are generally well-calibrated, though minor over- or under-confidence is observed in certain classes—again reflecting the effects of class imbalance and landscape heterogeneity (Xiao et al., 2024). Importantly, the low standard deviations observed in the 5-fold cross-validation results confirm that the model's performance is stable across different data partitions, which is crucial for practical applications and aligns with best practices recommended by recent remote sensing machine learning studies (Maxwell et al., 2018).

Feature importance analysis revealed that radar-based texture metrics (e.g., *VH Sum Average*; *VV Sum Variance*), optical vegetation indices (*Summer GNDVI Median*) and topographic variables (*SRTM Elevation* and *Terrain Slope*) played key roles in classification. This aligns with prior studies emphasizing the complementary nature of radar backscatter, optical indices, and terrain data for vegetation structure and type discrimination (Balzter et al., 2015; Mngadi et al., 2021). In particular, radar texture features have been shown to be especially valuable in distinguishing forest structural differences that may not be captured by optical data alone (Hanan et al., 2025).

Misclassifications in the model largely follow ecological and environmental gradients reflected in canopy structure, spectral behavior, and topographic context. The strongest confusions occur among loamy (class 1), rich/enriched (class 6), and beech–oak forests (class 7), where shared mixtures of oak, beech, and accessory broadleaves produce similar canopy textures and vegetation index responses; for example, enriched forests were frequently predicted as loamy or beech–oak forests, and beech–oak forests were misclassified as enriched. Oak–beech forests (class 4) also overlap with these types, reflecting their position along a moderate-fertility gradient, where stand structure and species composition transition gradually.

Our use of XGBoost for ecological forest type classification yields strong performance—echoing a growing consensus in vegetation mapping that gradient boosting frameworks often outperform other methods when using multi-source remote sensing data. For example, Shao et al. (2024) report that XGBoost exceeded Random Forest in urban impervious surface mapping, achieving an overall accuracy of 81% versus 77%, with its advantage attributed to its enhanced ability to leverage combined optical and SAR texture features. Similarly, Nguyen and Saha (2024) found that XGBoost surpassed Random Forest in forest carbon stock estimation tasks, showing superior predictive performance in 75% of comparative cases. These findings align with our results, where XGBoost consistently achieved accuracy around 88%.

Comparisons with deep learning approaches in the remote sensing literature highlight a different trade-off. Deep learning models—such as ResNet50 combined with XGBoost in ensemble frameworks—have demonstrated strong classification capabilities for high-resolution forest imagery (Kalinaki et al., 2023; Kwenda et al., 2023). However, purely deep architectures typically require large volumes of labeled data to achieve optimal performance (Yuan et al., 2020), whereas ensemble tree methods like XGBoost remain more robust in data-limited contexts thanks to their capacity to generalize effectively from structured tabular features derived through careful preprocessing (e.g., textural metrics, vegetation indices) (Belgiu and Drăguţ, 2016). Furthermore, deep learning approaches are generally designed to analyze sets of spatially coherent image tiles and learn hierarchical spatial patterns (Mishra et al., 2022). In contrast, many remote sensing applications—such as ours—work with a single large study area represented by pixel-level

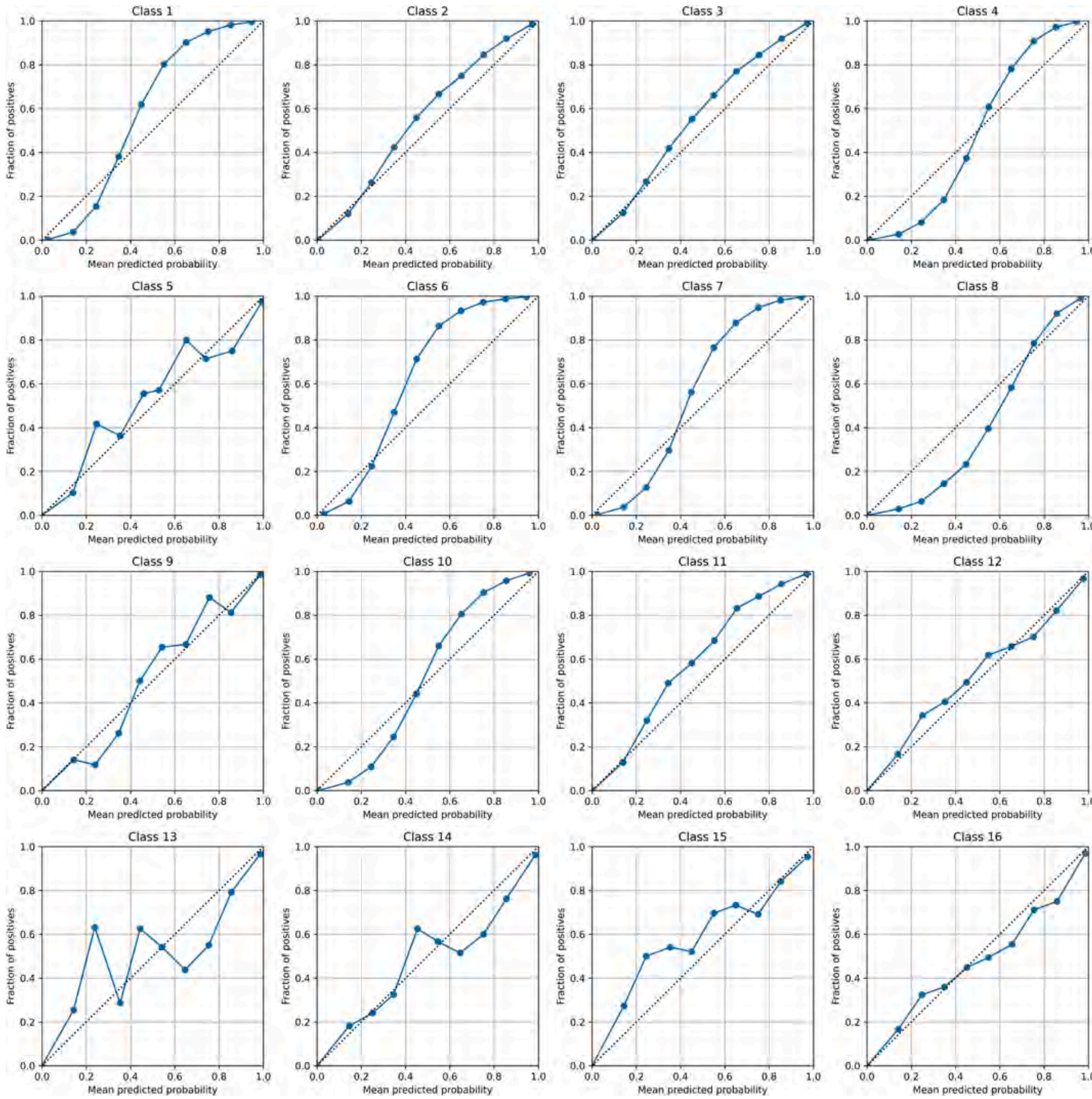

Fig. 9. Calibration plots for each target class (diagonal line is the perfect calibration).

feature vectors, where the primary challenge is to classify each pixel based on its descriptive attributes rather than on spatial neighborhood context. While deep learning methods may offer edge-case improvements (especially when incorporating spatial context from imagery), our results illustrate that, for structured feature inputs, XGBoost represents a high-performing, computationally efficient, and easily interpretable solution well suited for operational forest type classification.

Most studies in the remote sensing and forest mapping literature have focused on the classification of individual tree species or dominant canopy types, rather than broader ecological categories like those used in our work. Typical classification targets include species-level maps (e.g., oak, beech, fir, pine) (Axelsson et al., 2021; Liu et al., 2019) or coniferous–deciduous distinctions (Rüetschi, 2017), which are directly linked to clear spectral or textural differences observable in high-resolution imagery. In contrast, our study addresses a more complex task: classifying forest types defined by ecological and site characteristics—such as soil richness (rich/enriched), hydrological regime (drying, wet, waterlogged/streamside), or geological substrate (calcareous, acidic, skeletal/stony/dwarf). These classes do not always correspond to clear spectral signatures and often reflect subtle differences in site conditions, species composition, and forest structure. As a result, our approach extends beyond traditional species mapping by attempting to capture ecologically meaningful gradients and habitat types, which are critically important for biodiversity monitoring and forest ecosystem management.

However, several limitations should be acknowledged. First, there is a potential risk of overfitting, in which the model performs well on the training data but may not generalize reliably to new areas. Second, the

Table 4
Accuracy statistics on 5-fold cross validation.

ID	Precision mean	Precision std	Recall mean	Recall std	F1 mean	F1 std	No. of test pixels mean
1	0.8754	0.0024	0.8432	0.0034	0.859	0.0028	38421.2
2	0.903	0.0048	0.8916	0.0024	0.8973	0.0029	14541.8
3	0.9132	0.0033	0.9063	0.0039	0.9097	0.0009	8886.2
4	0.8289	0.0046	0.9277	0.0023	0.8755	0.0031	31312.8
5	0.9412	0.0104	0.9516	0.0102	0.9463	0.0085	541.2
6	0.9062	0.0018	0.8598	0.0029	0.8824	0.0023	107191.6
7	0.8606	0.0023	0.8743	0.0014	0.8674	0.0009	53762.2
8	0.8731	0.0021	0.9628	0.0013	0.9157	0.0015	15796.6
9	0.9387	0.0043	0.9488	0.009	0.9437	0.0059	1419
10	0.8919	0.0027	0.9386	0.0023	0.9147	0.0023	22026.4
11	0.9224	0.0038	0.8959	0.0043	0.9089	0.0024	8019.6
12	0.8802	0.0065	0.8861	0.0087	0.8831	0.0064	3396.4
13	0.8979	0.0074	0.8782	0.0186	0.8878	0.0096	466.2
14	0.8722	0.0121	0.8671	0.0084	0.8696	0.0068	809.8
15	0.8409	0.0191	0.7540	0.0109	0.7950	0.0112	948
16	0.9039	0.0039	0.9314	0.0039	0.9174	0.0035	2932
Overall							
accuracy	0.8829	0.0011	0.8829	0.0011	0.8829	0.0011	310471
macro avg	0.8906	0.0029	0.8948	0.0017	0.8921	0.0014	310471
weighted avg	0.8841	0.0011	0.8829	0.0011	0.8828	0.0011	310471

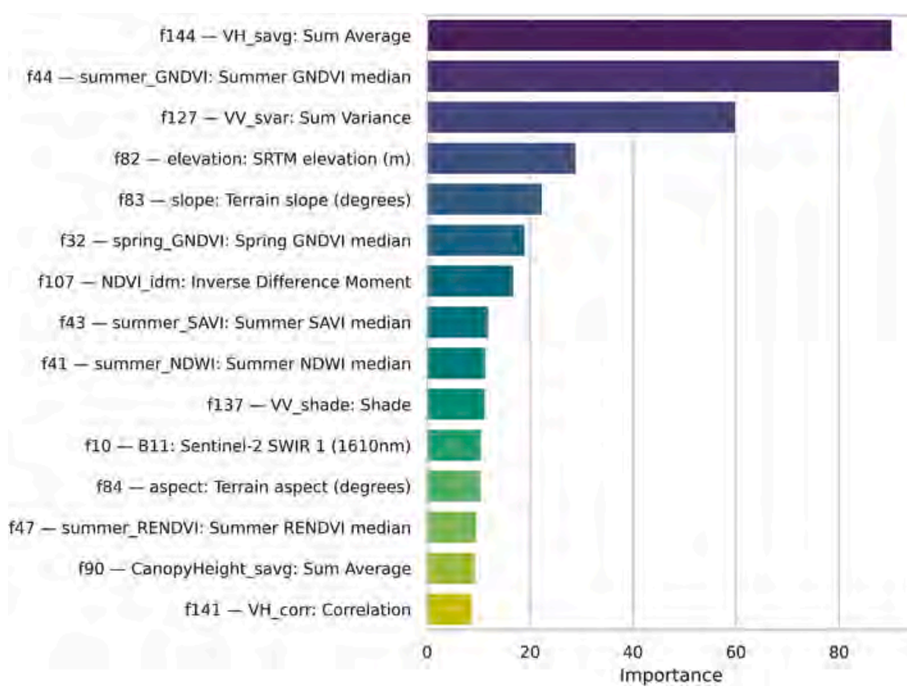

Fig. 10. Top 15 most important features (bands) by XGBoost classification.

model may rely heavily on topographic variables (e.g., elevation or slope) when distinguishing forest types; although these factors are correlated with ecological gradients, such relationships are not necessarily causal. Also, the canopy-height model and other remote-sensing products do not fully coincide temporally, which may introduce bias, although we assume the forest structure remained relatively stable during the study period. Although the study area covers 10,200 ha, its environmental conditions and forest composition may be locally specific, which could limit the generalizability of the model to other regions. Finally, the use of a random split may lead to overly optimistic performance estimates, as the model can exploit local similarities between training and testing data. Nevertheless, the focus of this study is on analyzing the ability to separate ecological forest classes based on remote sensing data, rather than producing the best generalizable model for predicting new areas.

Overall, this study demonstrates that combining multi sensor satellite data with class weighting strategies can effectively address the challenges of class imbalance and heterogeneity in forest mapping. The pipeline's reproducibility and use of open-source tools further enhance its applicability for large-scale or multi-temporal forest monitoring. Future work could explore advanced hyperparameter optimization, additional textural or structural features, training the model on new, unseen areas to test its ability to generalize, and integration with time-series analysis to further improve the classification of minority and transitional forest types.

5. Conclusion

In this study, we developed a machine learning pipeline to classify forest types based on multi-source remote sensing data, including

Sentinel-derived vegetation indices, SAR texture measures, and topographic variables. Using XGBoost, we achieved strong class separability, with an overall accuracy of approximately 88%, macro-averaged ROC AUC close to 0.995, and consistently high average precision across most classes. Notably, the most influential predictors included radar-derived texture metrics, seasonal vegetation indices, and terrain attributes, highlighting the value of integrating complementary data sources for forest classification. Model calibration metrics, such as a multiclass Brier score of 0.21 and Cohen's kappa of 0.86, alongside per-class calibration plots, further confirmed the reliability of predicted probabilities. The robustness of the approach was validated through five-fold cross-validation, which produced low variance in precision, recall, and F1-scores across folds, demonstrating stability even for minority classes.

These findings align with and extend previous research showing that combining SAR and optical data improves discrimination among complex forest communities, particularly when coupled with terrain information. Our open, reproducible workflow and feature analysis provide a practical and scalable framework that can support biodiversity monitoring, conservation planning, and large-scale forest mapping efforts. Future work could explore temporal dynamics, incorporate additional ecological covariates, test the ability to generalize, and benchmark alternative ensemble methods to further refine classification performance.

CRediT authorship contribution statement

Richard Kovárník: Writing – original draft, Visualization, Methodology, Investigation, Data curation, Conceptualization. **David Hampel:** Supervision, Methodology. **Jitka Janová:** Supervision.

Declaration of competing interest

The authors declare that they have no known competing financial interests or personal relationships that could have appeared to influence the work reported in this paper.

Acknowledgements

Supported by the grant IGA26-PEF-DP-003 of the IGA PEF MENDELU Grant Agency.

Data availability

Code and data are available at the following GitHub repository: https://github.com/xkovarn1/forest_types

References

Astola, H., Häme, T., Sirro, L., Molinier, M., Kilpi, J., 2019. Comparison of Sentinel-2 and Landsat 8 imagery for forest variable prediction in boreal region. Remote Sensing of Environment *223*, 257–273. https://doi.org/10.1016/j.rse.2019.01.019.

Axelsson, A., Lindberg, E., Reese, H., Olsson, H., 2021. Tree species classification using Sentinel-2 imagery and Bayesian inference. International Journal of Applied Earth Observation and Geoinformation *100*, 102318. https://doi.org/10.1016/j.jag.2021.102318.

Balzter, H., Cole, B., Thiel, C., Schmullius, C., 2015. Mapping CORINE land cover from Sentinel-1A SAR and SRTM digital elevation model data using random forests. Remote Sensing *7* (11), 14876–14898. https://doi.org/10.3390/rs71114876.

Belgiu, M., Drăguţ, L., 2016. Random forest in remote sensing: a review of applications and future directions. ISPRS journal of photogrammetry and remote sensing *114*, 24–31. https://doi.org/10.1016/j.isprsjprs.2016.01.011.

Bhagwat, R.U., Shankar, B.U., 2019. A novel multilabel classification of remote sensing images using XGBoost. In: 2019 IEEE 5th International Conference for Convergence in Technology (I2CT). IEEE. https://doi.org/10.1109/I2CT45611.2019.9033768.

Brownlee, J., 2016. XGBoost With python: Gradient Boosted Trees With XGBoost and scikit-learn. Machine Learning Mastery.

Chen, T., Guestrin, C., 2016. Xgboost: A scalable tree boosting system. In: Proceedings of the 22nd ACM Sigkdd International Conference on Knowledge Discovery and Data Mining, pp. 785–794. https://doi.org/10.1145/2939672.2939785.

Cohen, J., 1960. A coefficient of agreement for nominal scales. Educational and psychological measurement *20* (1), 37–46. https://doi.org/10.1177/001316446002000104.

Fang, G., Xu, H., Yang, S.-I., Lou, X., Fang, L., 2023. Synergistic use of Sentinel-1, Sentinel-2, and Landsat 8 in predicting forest variables. Ecological Indicators *151*, 110296. https://doi.org/10.1016/j.ecolind.2023.110296.

FAO, 2024. The State of the World's Forests 2024 – Forest-Sector Innovations Towards a More Sustainable Future. FAO, Rome. https://doi.org/10.4060/cd1211en.

Fassnacht, F.E., Latifi, H., Stereńczak, K., Modzelewska, A., Lefsky, M., Waser, L.T., Ghosh, A., 2016. Review of studies on tree species classification from remotely sensed data. Remote Sensing of Environment 186, 64–87. https://doi.org/10.1016/j.rse.2016.08.013.

Friedman, J.H., 2001. Greedy function approximation: a gradient boosting machine. Annals of statistics 1189–1232. Retrieved from. http://www.jstor.org/stable/2699986.

Glenn, W.B., et al., 1950. Verification of forecasts expressed in terms of probability. Monthly weather review 78 (1), 1–3.

Gorelick, N.A., Ilyushchenko, S., Thau, D., Moore, R., 2017. Google Earth Engine: planetary-scale geospatial analysis for everyone. Remote sensing of Environment *202*, 18–27. https://doi.org/10.1016/j.rse.2017.06.031.

Hammond, M.E., Pokorný, R., Dobrovolný, L., Hiitola, N., Friedl, M., 2020. Effect of gap size on tree species diversity of natural regeneration-case study from masaryk training forest enterprise Křtiny. Journal of Forest Science 66 (10), 407–419. https://doi.org/10.17221/78/2020-JFS.

Hanan, A., Khan, M., Fernandez-Anez, N., Arghandeh, R., 2025. DeepBioFusion: Multimodal deep learning based above ground biomass estimation using SAR and optical satellite images. Ecological Informatics, 103277. https://doi.org/10.1016/j.ecoinf.2025.103277.

Hansen, M.C., Potapov, P.V., Moore, R., Hancher, M., Turubanova, S.A., Tyukavina, A., et al., 2013. High-resolution global maps of 21st-century forest cover change. Science 342 (6160), 850–853. https://doi.org/10.1126/science.1244693.

He, H., Garcia, E.A., 2009. Learning from imbalanced data. IEEE Transactions on knowledge and data engineering 21 (9), 1263–1284. https://doi.org/10.1109/TKDE.2008.239.

Kalinaki, K., Malik, O.A., Lai, D.T., Sukri, R.S., Wahab, R.B., 2023. Spatial-temporal mapping of forest vegetation cover changes along highways in Brunei using deep learning techniques and Sentinel-2 images. Ecological Informatics 77, 102193. https://doi.org/10.1016/j.ecoinf.2023.102193.

Kaur, H., Pannu, H.S., Malhi, A.K., 2019. A systematic review on imbalanced data challenges in machine learning: applications and solutions. ACM Computing Surveys (CSUR) 52 (4), 1–36. https://doi.org/10.1145/334344.

Kovárník, R., Janová, J., 2025. Validation of sentinel 2 based machine learning models for Czech National Forest Inventory. Ecological Informatics *87*, 103133. https://doi.org/10.1016/j.ecoinf.2025.103133.

Kowalski, K., Senf, C., Hostert, P., Pflugmacher, D., 2020. Characterizing spring phenology of temperate broadleaf forests using Landsat and Sentinel-2 time series. International Journal of Applied Earth Observation and Geoinformation *92*, 102172. https://doi.org/10.1016/j.jag.2020.102172.

Kozhoridze, G., Orlovsky, N., Orlovsky, L., Blumberg, D.G., Golan-Goldhirsh, A., 2016. Remote sensing models of structure-related biochemicals and pigments for classification of trees. Remote Sensing of Environment 186, 184–195. https://doi.org/10.1016/j.rse.2016.08.024.

Kwenda, C., Gwetu, M.V., Fonou-Dombeu, J.V., 2023. Forest image classification based on deep learning and XGBoost algorithm. In: International Conference on Computational Science. Springer, pp. 217–229. https://doi.org/10.1007/978-3-031-36027-5_16.

Liu, J., Wang, X., Wang, T., 2019. Classification of tree species and stock volume estimation in ground forest images using Deep Learning. Computers and Electronics in Agriculture *166*, 105012. https://doi.org/10.1016/j.compag.2019.105012.

Ma, M., Liu, J., Liu, M., Zeng, J., Li, Y., 2021. Tree species classification based on Sentinel-2 imagery and random forest classifier in the eastern regions of the Qilian Mountains. Forests *12* (12), 1736. https://doi.org/10.3390/f12121736.

Mašínová, T., Bahnmann, B.D., Větrovský, T., Tomšovský, M., Merunková, K., Baldrian, P., 2017. Drivers of yeast community composition in the litter and soil of a temperate forest. FEMS Microbiology Ecology 9 (2), fiw223. https://doi.org/10.1093/femsec/fiw223.

Maxwell, A.E., Warner, T.A., Fang, F., 2018. Implementation of machine-learning classification in remote sensing: an applied review. International journal of remote sensing 39 (9), 2784–2817. https://doi.org/10.1080/01431161.2018.1433343.

Mishra, B., Dahal, A., Luintel, N., Shahi, T.B., Panthi, S., Pariyar, S., Ghimire, B.R., 2022. Methods in the spatial deep learning: current status and future direction. Spatial Information Research 30 (2), 215–232. https://doi.org/10.1007/s41324-021-00425-2.

Miura, S., Amacher, M., Hofer, T., San-Miguel-Ayanz, J., Thackway, R., et al., 2015. Protective functions and ecosystem services of global forests in the past quarter-century. Forest Ecology and Management *352*, 35–46. https://doi.org/10.1016/j.foreco.2015.03.039.

Mngadi, M., Odindi, J., Peerbhay, K., Mutanga, O., 2021. Examining the effectiveness of Sentinel-1 and 2 imagery for commercial forest species mapping. Geocarto International *36* (1), 1–12. https://doi.org/10.1080/10106049.2019.1585483.

Mohammadpour, P., Viegas, D.X., Viegas, C., 2022. Vegetation mapping with random forest using sentinel 2 and GLCM texture feature—a case study for Lousã region, Portugal. Remote Sensing 14 (18), 4585. https://doi.org/10.3390/rs14184585.

Nguyen, A., Saha, S., 2024. Machine learning and multi-source remote sensing in forest carbon stock estimation: a review. arXiv Preprint. https://doi.org/10.48550/arXiv.2411.17624 arXiv:2411.17624.

Niculescu-Mizil, A., Caruana, R., 2005. Predicting good probabilities with supervised learning. In: Proceedings of the 22nd international conference on Machine learning, pp. 625–632.
Pu, R., 2021. Mapping tree species using advanced remote sensing technologies: A state-of-the-art review and perspective. *Journal of remote sensing.* https://doi.org/10.34133/2021/9812624.
Rüetschi, M.a, 2017. Using multitemporal sentinel-1 c-band backscatter to monitor phenology and classify deciduous and coniferous forests in northern switzerland. Remote Sensing *10* (1), 55. https://doi.org/10.3390/rs10010055.
Sahin, E.K., 2020. Assessing the predictive capability of ensemble tree methods for landslide susceptibility mapping using XGBoost, gradient boosting machine, and random forest. SN Applied Sciences 2 (7), 1308. https://doi.org/10.1007/s42452-020-3060-1.
Seidl, R., Thom, D., Kautz, M., Martin-Benito, D., Peltoniemi, M., Vacchiano, G., et al., 2017. Forest disturbances under climate change. Nature Climate Change *7* (6), 395–402. https://doi.org/10.1038/nclimate3303.
Shao, Z., Ahmad, M.N., Javed, A., 2024. Comparison of random forest and XGBoost classifiers using integrated optical and SAR features for mapping urban impervious surface. Remote Sensing 16 (4), 665. https://doi.org/10.3390/rs16040665.
Song, X.-P., Huang, W., Hansen, M.C., Potapov, P., 2021. An evaluation of Landsat, Sentinel-2, Sentinel-1 and MODIS data for crop type mapping. Science of Remote Sensing 3, 100018. https://doi.org/10.1016/j.srs.2021.100018.
Sunde, M., Diamond, D., Elliott, L., 2024. Ecological systems classification: integrating machine learning, ancillary modeling, and Sentinel-2 satellite imagery. Remote Sensing *16* (23), 4440. https://doi.org/10.3390/rs16234440.
Tolan, J., Yang, H.-I., Nosarzewski, B., Couairon, G., Vo, H.V., Brandt, J., et al., 2024. Very high resolution canopy height maps from RGB imagery using self-supervised vision transformer and convolutional decoder trained on aerial lidar. Remote Sensing of Environment 300, 113888. https://doi.org/10.1016/j.rse.2023.113888.
Viewegh, J., 2012. Czech forest ecosystem classification. Journal of Forest Science *49* (2), 74–82.
Wan, H., Tang, Y., Jing, L., Li, H., Qiu, F., Wu, W., 2021. Tree species classification of forest stands using multisource remote sensing data. Remote Sensing *13* (1), 144. https://doi.org/10.3390/rs13010144.
Wulder, M.A., Loveland, T.R., Roy, D.P., Crawford, C.J., Masek, J.G., Woodcock, C.E., et al., 2019. Current status of Landsat program, science, and applications. Remote sensing of environment 225, 127–147. https://doi.org/10.1016/j.rse.2019.02.015.
Xiao, Y., Huang, J., Weng, W., Huang, R., Shao, Q., Zhou, C., Li, S., 2024. Class imbalance: a crucial factor affecting the performance of tea plantations mapping by machine learning. International Journal of Applied Earth Observation and Geoinformation *129*, 103849. https://doi.org/10.1016/j.jag.2024.103849.
Yuan, Q., Shen, H., Li, T., Li, Z., Li, S., Jiang, Y., et al., 2020. Deep learning in environmental remote sensing: achievements and challenges. Remote sensing of Environment *241*, 111716. https://doi.org/10.1016/j.rse.2020.111716.
Zhao, D., Zhen, J., Zhang, Y., Miao, J., Shen, Z., Jiang, X., Wu, G., 2023. Mapping mangrove leaf area index (LAI) by combining remote sensing images with PROSAIL-D and XGBoost methods. Remote Sensing in Ecology and Conservation *9* (3), 370–389. https://doi.org/10.1002/rse2.315.
Zhen, J., Mao, D., Shen, Z., Zhao, D., Xu, Y., Wang, J., Ren, C., 2024. Performance of xgboost ensemble learning algorithm for mangrove species classification with multisource spaceborne remote sensing data. Journal of Remote Sensing *4*, 0146. https://doi.org/10.34133/remotesensing.0146.
Zhou, G., Ni, Z., Zhao, Y., Luan, J., 2022. Identification of bamboo species based on Extreme Gradient Boosting (XGBoost) using Zhuhai-1 orbita hyperspectral remote sensing imagery. Sensors *22* (14), 5434. https://doi.org/10.3390/s22145434.